JOC The Journal of Organic Chemistry

pubs.acs.org/joc Article

Shortwave Infrared Absorptive and Emissive Pentamethine-Bridged Indolizine Cyanine Dyes

David Ndaleh, Cameron Smith, Mahesh Loku Yaddehige, Abdul Kalam Shaik, Davita L. Watkins, Nathan I. Hammer, and Jared H. Delcamp*

Cite This: J. Org. Chem. 2021, 86, 15376−15386 Read Online

ACCESS | Metrics & More | Article Recommendations | Supporting Information

ABSTRACT: Shortwave infrared (SWIR)-emitting small molecules are desirable for biological imaging applications. In this study, four novel pentamethine indolizine cyanine dyes were synthesized with *N*,*N*-dimethylaniline-based substituents on the indolizine periphery at varied substitution sites. The dyes are studied via computational chemistry and optical spectroscopy both in solution and when encapsulated. Dramatic spectral shifts in the absorption and emission spectrum wavelengths with added donor groups are observed. Significant absorption and emission with an emissive quantum yield as high as 3.6% in the SWIR region is possible through the addition of multiple donor groups per indolizine.

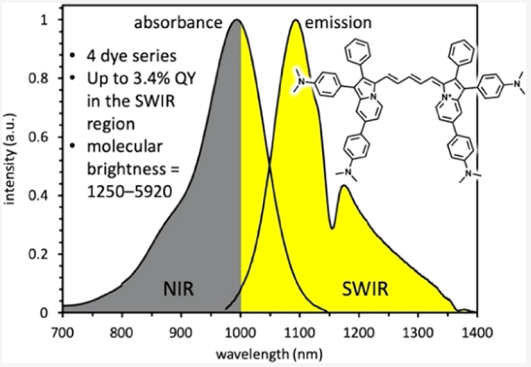

INTRODUCTION

The need for molecular shortwave infrared (SWIR) emissive materials for biological imaging is apparent.[1−6] In vivo SWIR (1000−2000 nm or near-infrared-II, NIR-II) imaging offers deeper tissue penetration, low tissue photon scattering, and low autofluorescence of biological medium.[1−6] These advantages lead to high signal-to-noise ratios and high contrast image visualization at centimeter depths in anatomical tissue.[7] Cyanines are well-known as an exceptionally strong absorbing and emitting class of materials with high molecular brightness (MB, where MB = $\varepsilon \times \phi$, with ε being molar absorptivity and ϕ being the emission quantum yield) values in the near-infrared (NIR) region.[8,9] MB values are related to the amount of the emissive probe that is needed to rapidly generate a high-quality image with higher MB value materials allowing for the use of lower probe quantities. Additionally, cyanines are often relatively nontoxic compared to many emissive materials in the NIR and SWIR regions, with cellular component level targeting possible.[6,9−13]

Relatively few polymethine cyanines have been reported to both significantly absorb and emit in the SWIR region (see example references).[14−21] Recently, we reported a cyanine dye utilizing a novel indolizine donor group linked to a pentamethine bridge absorbing and emitting in the 800−900 nm region with a ϕ of 3.5% and a good MB of 5800.[22,23] Indolizine is a nitrogen-based proaromatic heterocyclic donor similar to oxygen-based pyrilium/chromenylium donors which have shown some of the furthest penetration into the SWIR region.[14−16] Interestingly, an indolizine *penta*methine-bridged dye absorbs and emits at a similar wavelength to pyrilium-based *hepta*methine-bridged dyes, which is likely due to the stronger electron donation strength of nitrogen when compared to oxygen (Figure 1). Compared to a non-proaromatic nitrogen-based indoline donor with a *hepta*methine-bridged cyanine, longer wavelengths are accessed with the indolizine donor group on a *penta*methine-bridged cyanine (Figure 1). Inspired by findings that pyrilium and thiopyrylium-based polymethine cyanine dye emission wavelengths can be shifted further into the SWIR region by the use of amine donor groups on the periphery, a similar strategy is evaluated with a pentamethine indolizine dye.[16,18] Thus, the synthesis of two dyes with strategically added amine peripheral donor groups was pursued. The addition of multiple amine donor groups to the periphery of a single indolizine heterocycle was also pursued to evaluate the cumulative effect of added donors (Figure 1).

RESULTS AND DISCUSSION

The most attractive positions for the addition of amine donor substitutions were selected based on the position of the highest occupied molecular orbital (HOMO) as determined by density functional theory (DFT) calculations at the B3LYP/6-

Received: August 9, 2021
Published: October 14, 2021

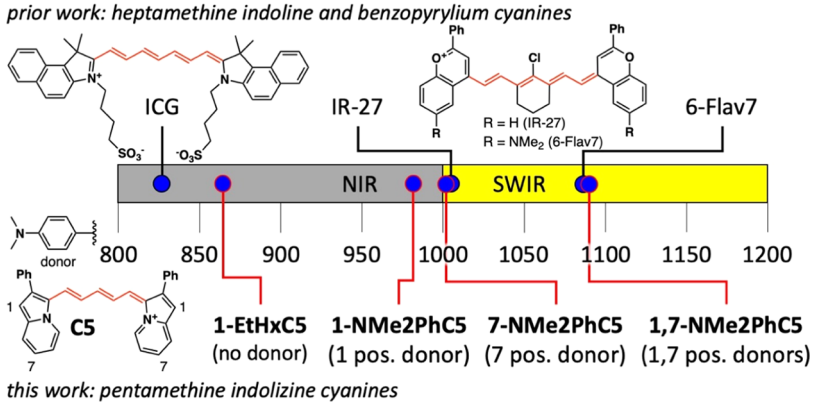

Figure 1. Pentamethine indolizine cyanine dyes compared to known heptamethine cyanine peak emission wavelengths.

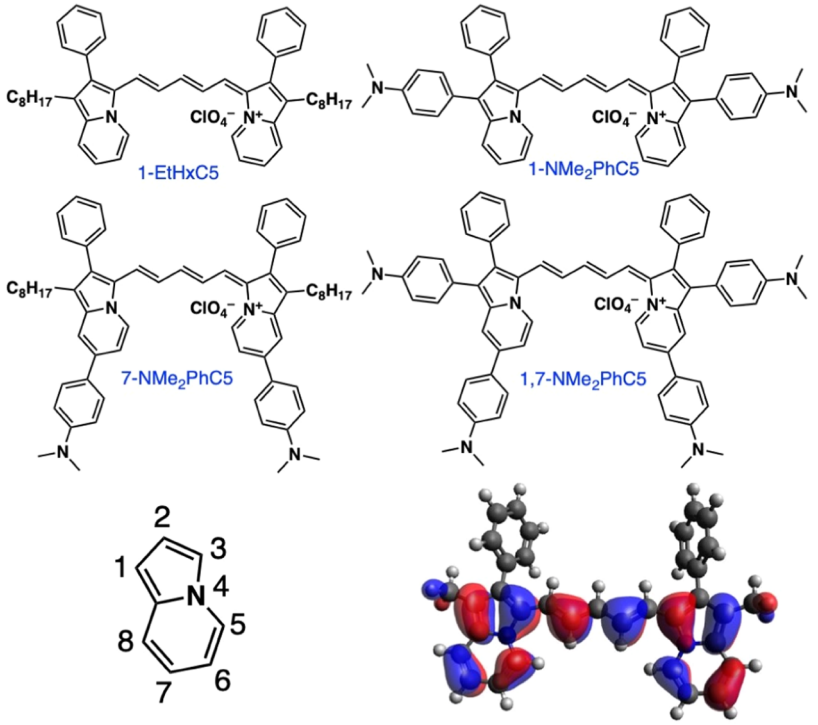

Figure 2. Structures of the target dyes with the HOMO orbital of 1-EtHxC5 shown. The 2-ethylhexyl groups (noted as C_8H_{17}) are truncated to methyl groups during computational studies.

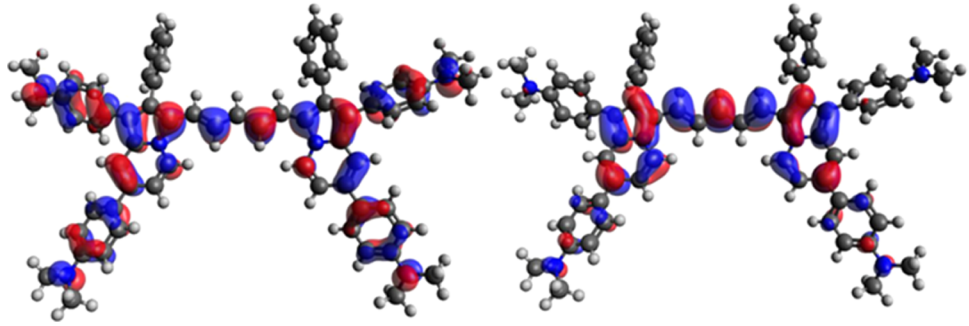

Figure 3. Example HOMO (left) and LUMO (right) orbitals for **1,7-NMe2PhC5**. See the SI for the orbitals with the remaining dyes.

311G(d,p) level of theory[24−26] with dichloromethane as an implicit solvent via a polarizable continuum model.[27−29] Substitutions at the HOMO orbital positions with electron-rich functionality are expected to extend HOMO orbital delocalization. The most synthetically accessible positions with large HOMO coefficients are the 1 and 7 positions of indolizine (Figure 2). Thus, a series of dyes were targeted with no amine donor on the 1 or 7 position and *N*,*N*-dimethylani-

https://doi.org/10.1021/acs.joc.1c01908
J. Org. Chem. 2021, 86, 15376−15386

Scheme 1. Synthetic Scheme to Access the Pentamethine Indolizine Cyanine Dyes

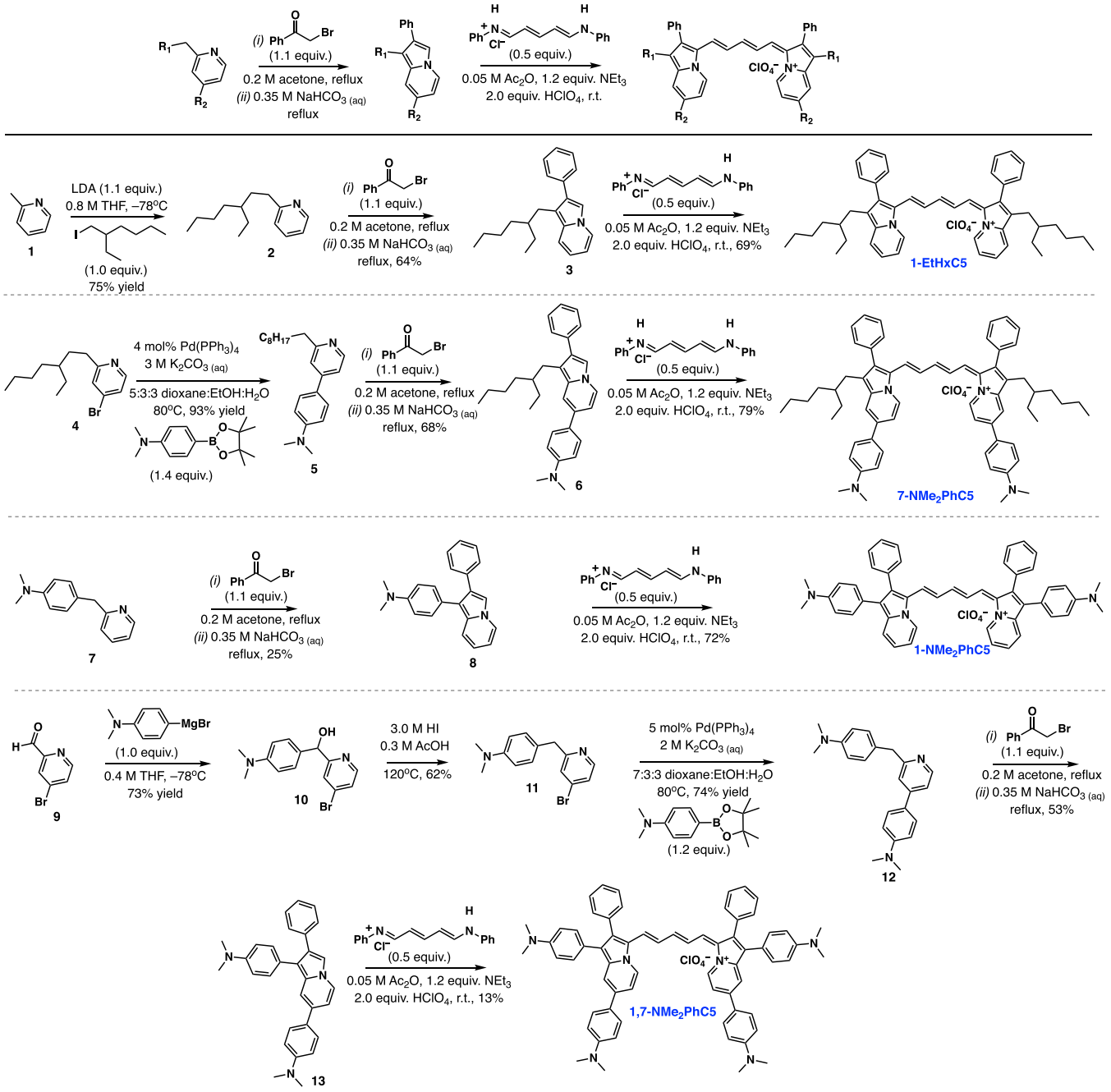

line-derived donors at either or both of the 1 and 7 positions. This approach allows for analysis of the influence of a strong donor at both positions independently and the analysis of cumulative donor strength.

The target dyes were computationally evaluated to probe the involvement of the added donor groups on the frontier molecular orbitals of the dyes. In all cases, the HOMO orbital was delocalized and is observed to be present on the pentamethine bridge, indolizine heterocycles, and *N,N*-dimethylaniline-based donors when present (see Figure 3 for **1,7-NMe2PhC5** as an example and Figure S3 for the remaining dyes). The lowest unoccupied molecular orbital (LUMO) is primarily positioned on the pentamethine bridge and indolizine heterocycle with a lesser contribution on *N,N*-dimethylanaline-based donors. The positioning of the HOMO on amine donor groups is a strong indicator that these groups will play a significant role in tuning the optical properties of the target dyes. Importantly, the addition of donor groups does not seem to perturb the $\pi-\pi^*$ HOMO to LUMO transition character substantially since both orbitals remain delocalized with significant overlap.

Time-dependent (TD)-DFT analysis reveals that the HOMO to LUMO transition is strong for all of the dye (>1.0 oscillator strength), which is consistent with typical cyanine dye oscillator strengths (Table S3).[18] Addition of *N,N*-dimethylaniline-based donor groups shifts the vertical transition energy toward longer wavelength from 1.99 to 1.46 eV with the following order of decreasing vertical transition energies observed: **1-EtHxC5> 7-NMe2PhC5> 1-NMe2PhC5> 1,7-NMe2PhC5**. Substitutions at both the 1

https://doi.org/10.1021/acs.joc.1c01908
J. Org. Chem. 2021, 86, 15376−15386

and 7 positions of indolizine result in significant tunability of the vertical transition energy (0.37−0.50 eV shift toward lower energy). Additionally, cumulative effects are noted with the dual donor dye (**1,7-NMe2PhC5**) having the lowest energy vertical transition.

The target dyes were synthesized by first installing aniline-based donor groups on pyridine derivatives at the carbon positions that lead to the desired indolizine substitution patterns and then cyclizing the indolizine heterocycle (Scheme 1). The pyridine derivatives (**2**, **5**, **7**, and **12**) were all alkylated with 2-bromoacetophenone and cyclized via the addition of a base to give indolizines (**3**, **6**, **8**, and **13**) in modest to good yields. Intriguingly, exceptionally electron-rich building blocks such as triple nitrogen donor **13** is isolatable with Al_2O_3 chromatography and can be safely stored prior to use. The target dyes were formed via condensation reactions with indolizines (**3**, **6**, **8**, and **13**) and *N*-((1*E*,3*E*,5*E*)-5-(phenylimino)penta-1,3-dien-1-yl)aniline monohydrochloride in modest to good yields. Notably, the dyes were shelf stable as solids for multiple months under ambient conditions with no signs of instability.

The absorption characteristics of the pentamethine-bridged indolizine cyanine dyes were examined to understand the effect of *N*,*N*-dimethylaniline-based substituents at the different positions of indolizine. The parent dye (**1-EtHxC5**) has a narrow absorption band (full width at half-maximum, FWHM, of 1003 cm^{-1}) with an absorption maxima (λ_{max}^{abs}) at 827 nm in dimethylsulfoxide (DMSO, Figure 4, Table 1). A prominent shoulder peak at 725 nm is also present, which is assigned as a vibronic feature.[30] The λ_{max}^{abs} of **1-NMe2PhC5** is shifted 65 nm toward longer wavelengths with a broader absorption curve (FWHM of 1791 cm^{-1}) than the parent dye. This broadened absorption is accompanied by a diminished molar absorptivity (ε) to 80 000 M^{-1} cm^{-1} from the 171 000 M^{-1} cm^{-1} value observed with **1-EtHxC5**. These changes in peak width and ε are correlated with DFT geometry optimizations, showing a significant dihedral angle (48°) between the *N*,*N*-dimethylaniline donor in the 1 position and the pentamethine bridge (Figure S4).

7-NMe2PhC5 has a λ_{max}^{abs} of 940 nm, which is a 113 nm shift toward long wavelength relative to **1-EtHxC5**. Additionally, the absorption band of the dye narrows with an FWHM of 785 cm^{-1} and the ε value decreases slightly to 165 000 M^{-1} cm^{-1}. Combining these two approaches result in a λ_{max}^{abs} of 970 nm with **1,7-NMe2PhC5**. The absorption curve onset of **1,7-NMe2PhC5** was found to extend substantially into the SWIR region to 1088 nm using a computer-generated inflection point method and tailing to ∼1150 nm.[31] Thus, both the 1 and 7 positions of indolizine show a dramatic tunability of the λ_{max}^{abs} value with cumulative effects observed if both positions are simultaneously substituted with amine donor groups. These substitutions shifted the absorption spectrum onset from the NIR region at 877 nm with no donor groups to the SWIR region at 1088 nm with two donor groups. Notably, all of the pentamethine indolizine-based cyanines in this series are 26−170 nm more red-shifted relative to popular heptamethine indoline cyanine dyes such as indocyanine green (**ICG**),[32,33] **IR-780**,[34,35] and **IR-820**.[36,37] Additionally, many heptamethine cyanines such as **IR26** suffer from signal attenuation and broadening in polar solvents (e.g., DMSO).[18] However, similar trends and absorption curve shapes are observed in dimethylsulfoxide, dichloromethane, acetonitrile, and tetrahydrofuran for all of the indolizine cyanine dyes studied, suggesting that these dyes will remain emissive in an array of environments (Figure S5, Tables S4 and S5).

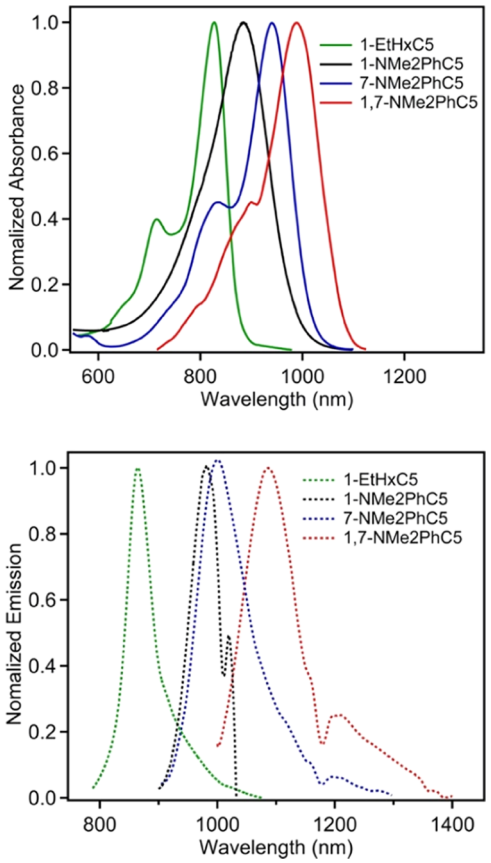

Figure 4. Normalized absorption (top) and emission (bottom) in DMSO (fit with 0.1 LOESS function). A ten micromolar solution of each dye was used to collect all emission data, exciting at 785 nm (for **1-EtHxC5** and **1-NMe2PhC5**) and 950 nm (for **7-NMe2PhC5** and **1,7-NMe2PhC5**).

The emissive properties of the dyes were examined with regard to the emission curve shape, emission maxima (λ_{max}^{em}), and ϕ values for each of the dyes. The λ_{max}^{em} of **1-EtHxC5** is at 864 nm in DMSO with a ϕ of 3.4% for a MB of 5800 (ref dye **IR-820**;[37] ϕ = 0.044). The emission curve mirrors the absorption curve which suggests the shoulder feature at ∼725 nm in the absorption spectrum is vibronic. **1-NMe2PhC5** has a λ_{max}^{em} of 987 nm with a low, negligible ϕ with a very low-intensity emission. The very weak emission curve is observable on a CCD detector; however, the expected smooth tailing of the emission curve is not observed, presumably due to the detection limits of the instrument being reached (Figure S6). The λ_{max}^{em} of **7-NMe2PhC5** is in the SWIR region at 1001 nm in DMSO with a ϕ of 3.6% for an MB of 5900 (ref dye **IR-1061**;[38] ϕ = 0.017). The emission onset is observed at ∼1300 nm. The dual donor **1,7-NMe2PhC5** dye has a λ_{max}^{em} of 1087 nm with a ϕ value of 1.0% (ref dye **IR-1061**). This dye absorbs and emits in the SWIR region with emission tailing until ∼1400 nm. Thus, the combined donor approach was able to shift the parent dye absorption (827 nm) and emission (864 nm) from the NIR region to the SWIR region with the peak absorption just outside the SWIR region (970 nm) but with an onset well within the SWIR region. Compared to benchmark materials

https://doi.org/10.1021/acs.joc.1c01908
J. Org. Chem. 2021, 86, 15376−15386

Table 1. Photophysical Data of the Synthesized Pentamethine Indolizine Cyanines in DMSO

dye	λ_{max}^{abs} (nm)	λ_{max}^{em} (nm)	ϕ (%)	ε (M^{-1} cm^{-1})	MB	SS (eV)
1-EtHxC5	827	864	3.4	171 000	5800	0.06
1-NMe2PhC5	895	982	N/A	80 000	N/A	0.12
7-NMe2PhC5	940	1001	3.6	165 000	5900	0.08
1,7-NMe2PhC5	970	1087	1.0	120 000	1200	0.14

such as IR-27 and 6-Flav7 in the SWIR region, the dyes in this report have a significantly higher molecular brightness (Figure S12). The Stokes shifts (the difference between λ_{max}^{abs} and λ_{max}^{em} energetically) were found to be closely grouped in energy from 0.06 to 0.14 eV. The magnitude of the Stokes shift of an emissive material is directly proportional to the reorganization energy of the fluorophore. Introduction of the donor group at the 7 position introduces a modest amount of increased reorganization energy (to 0.08 eV from 0.06 eV), while substitution at the more sterically hindered 1 position of indolizine results in double the Stokes shift energy (0.14 eV). The Stokes shifts, however, are modest compared to charge transfer dyes.[39]

Encapsulation studies were undertaken with **1,7-NMe2PhC5** using PAMAM-PCL,[40] DSPE-mPEG2000,[19] and Pluronic F-127 (PF-127)[41] to allow for emission studies in water since the dyes are not soluble in pure water and these encapsulation agents have shown excellent emissive properties with NIR/SWIR dyes previously (Figure 5, see the SI for

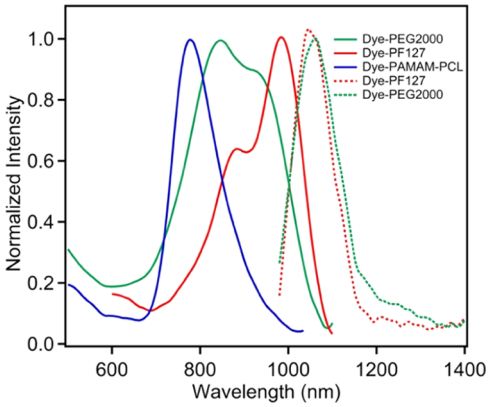

Figure 5. Normalized absorption (solid line) and emission (dash line) of encapsulated **1,7-NMe2PhC5** in water (emission curves fit with a 0.1 LOESS function).

structures, particle sizes, and encapsulation efficiencies). Interestingly, three separate absorption curves were observed with the three encapsulation methods. Dye encapsulated with PAMAM-PCL was found to give a significantly blue-shifted absorption curve (λ_{max}^{abs} = 780 nm) in water relative to the dye in DMSO (190 nm blue shift). This blue shift may be a result of aggregation such as when H-aggregates are formed. To probe this theory, all of the nanoencapsulated dyes were de-encapsulated by freeze-drying the samples and redissolving the dyes in organic solvent, which gives very similar spectrum to the dyes prior to encapsulation (Figures S9–S11). Dye-PAMAM-PCL nanoparticles were found to be nonemissive; however, upon rupturing nanoparticles, the dye was found to remain with optical properties unperturbed. This on/off behavior may have value in monitoring drug release mechanisms from dendrimer encapsulated materials. The Dye-DSPE-mPEG2000 micelle shows two absorption features at 855 and 950 nm in water. Emission is observed at 1063 nm. Presumably, the higher energy feature is a nonemissive aggregate, and the lower energy feature is monomeric emission. The Dye-PF-127 micelle shows an absorption profile similar to that of the monomeric dye in DMSO, with λ_{max}^{abs} at 991 nm and a shoulder peak at 878 nm. The emission maximum of this material is at 1055 nm in water, and the material remains emissive for at least a month without substantial change to the absorption curve profile making this an attractive material for biological imaging in NIR/SWIR regions (Figure S8).

CONCLUSIONS

Four indolizine pentamethine cyanine dyes were synthesized with *N*,*N*-dimethylaniline-based donor groups at varied positions on indolizine rings. Computational analysis guided the target dye selection with significant HOMO orbital contribution observed at the synthetically accessible 1 and 7 positions on indolizine. The absorption and emission studies show that this dye design strategy leads to a high tunability of the peak absorption (143 nm shift possible) and emission (223 nm shift possible) wavelength values. The parent dye with no aniline-based donor absorbs and emits primarily in the NIR region; however, through the use of multiple donor groups on each indolizine heterocycle, the absorption and emission are extended into the SWIR region. Despite the shorter methine chain, indolizine pentamethine cyanines reported herein are more red-shifted than typical heptamethine indoline cyanine dyes. A good emission quantum yield of 1% is observed in the SWIR region. The exceptional tunability of this system is attractive for multiplex imaging applications, and access to the SWIR region is attractive for a number of in vivo applications. The observed SWIR emission near 1100 nm and the relative ease of synthesis of these stable materials suggest that this design is attractive for further studies. The strategy of adding multiple donors for a cumulative effect on the spectroscopic properties of the dye is an approach that will likely be of value to many classes of dyes, especially those that use proaromatic donor groups (e.g., pyridinium, pyrylium, etc.). We have also demonstrated the encapsulation of **1,7-NMe2PhC5** in polymeric nanoparticles for emission in aqueous environments. Future studies are focused on bioconjugation strategies and synthetic approaches to access longer wavelength absorbing and emitting indolizine polymethine cyanine dyes.

EXPERIMENTAL SECTION

General Experimental Information. All commercially obtained reagents and solvents were used as received without further purification. *N*-((1*E*,3*E*,5*E*)-5-(phenylimino)penta-1,3-dien-1-yl)-aniline monohydrochloride was purchased from TCI America, and 2-bromo-1-phenylethan-1-one was purchased from Alfa Aesar. 4-Bromo-2-(3-ethylheptyl)pyridine (**4**) is a known compound, which was synthesized according to the literature procedure with ^{1}H NMR data collected in agreement with the reported values.[42] The final dyes were isolated as perchlorate salts, and care is advised while handling all perchlorate salts, especially when concentrating to a solid. The dyes

https://doi.org/10.1021/acs.joc.1c01908
J. Org. Chem. 2021, 86, 15376–15386

described herein were well behaved in our hands. Thin-layer silica gel chromatography (TLC) was conducted with either Sorbent Technologies, Inc. glass-backed 250 μm Silica Gel XHL TLC plates or with Merck KGaA precoated TLC silica gel 60 F254 aluminum sheets and both utilized a UV254 indicator. ^{1}H and ^{13}C NMR spectra were recorded on a Bruker Avance-300 (300 MHz) spectrometer and a Bruker Avance-400 (400 MHz) spectrometer and are reported in ppm using solvent as an internal standard ($CDCl_3$ at 7.26 ppm and DMSO at 2.50 ppm). Data are reported as s = singlet, d = doublet, t = triplet, m = multiplet, and br = broad; coupling constant(s) are in Hz; and integration. UV−vis−NIR spectra were measured with a Cary 5000 UV−vis−NIR spectrometer. All molar absorptivity measurements are repeated in triplicate with an error of ±2000 M^{-1} cm^{-1} observed for **1-EtHxC5** (1.1% error) and **7-NMe2PhC5** (1.2% error). An error of ±1000 M^{-1} cm^{-1} is observed for the molar absorptivity measurements on **1-NMe2PhC5** (1.3%) and **1,7-NMe2PhC5** (0.8% error). For electrospray ionization (ESI) high-resolution mass spectrometry (HRMS), quadruple-TOF was used to obtain the data both in positive and negative modes with a Waters Synapt HDMS. The mass analyzer was set to the 200−2000 Da range. Infrared spectra were recorded with a Bruker α FTIR spectrometer and spectra processed on OPUS 6.5 software. Elemental analysis was conducted by Atlantic Microlabs. The high-performance liquid chromatography (HPLC) system used is an Agilent 1100 series with an Agilent Zorbax Eclipse Plus C18 column (3.5 μm, 2.1 × 100 mm) stationary phase at ambient temperature. Mobile phases and flow rates are listed below HPLC figures. The emission data of **1-EtHxC5** and **1-NMe2PhC5** were collected using Horiba LabRAM HR Evolution Raman spectrometer with a 785 nm excitation laser at 1.25 mW of power with a hole size of 100 μm and a 600 g/mm. The detector used was a silicon-based CCD detector, with **IR820** as the reference dye (ϕ = 0.044).[37] For **7-NMe2PhC5** and **1,7-NMe2PhC5**, emission data were measured using a Horiba PTI QuantaMaster QM-8075-21 fluorometer using a 950 nm excitation source and an excitation slit width of 4.61 mm and an emission slit width of 5.76 mm; **IR-1061** was the reference dye (ϕ = 0.017).[38] Rectangular 10 mm path cuvettes were used for all fluorescence measurements and sealed under N_2 so that all measurements were taken under an inert atmosphere. The photoluminescent quantum yields (PLQY) of the dyes in different solvents were determined using the integrated emission intensity values (summation of all data points Y-values using Microsoft Excel and their absorbances were >0.1 at the excitation wavelength for all of the dyes) using the relative quantum yield equation:[43]

$$\Phi_s = \Phi_R \frac{E_s A_R(\eta_s^2)}{E_R A_s(\eta_R^2)}$$

where Φ denotes the quantum yield, E refers to integrated emission intensity, A is the equation represents $1-10^{-A}$ with the superscript A being the absorbance at the excitation wavelength, η is the refractive index of the solvent, s is sample, and R is the reference standard chosen for quantum yield studies. For PLQY measurements reported in Table 1 of the manuscript, a relatively high degree of experimental uncertainty is reported at 20 and 30% of PLQY for **1-EtHxC5** and **7-NMe2PhC5**/**1,7-NMe2PhC5**, respectively. This originates from the degree of uncertainty reported for **IR1061**[38] and **ICG**,[44] which was used to calculate the PLQY of **IR820.**[37] Although the minimal degree of uncertainty for relative PLQY is referenced as being 2% for the experimental method used in this study,[45] it is not fundamentally possible to be more certain than the least certain portion of the calculation.

General Computational Information. Molecules were drawn in ChemDraw (19.1.0.5) and saved as an MDL Molfile. These geometries were then optimized with the MMFF94 force field via Avogadro (1.2.0). Dihedral angles about noncyclic single bonds were set to between 0 and 90 degrees manually to avoid local minima conformations. Accurate geometry optimization was performed sequentially by DFT using Guassian 16[46] with the B3LYP functional[24,25] with the following basis sets: first 3-21g, second 6-31g (d,p),[47,48] and finally 6-311g (d,p)[26] all in dichloromethane as a polarizable continuum model (PCM).[27−29] TD-DFT computations were performed with optimized geometries with the B3LYP functional and 6-311g (d,p) basis set to compute vertical transition energies and oscillator strengths.

Synthetic Procedures. *2-(3-Ethylheptyl)pyridine (**2**).* To a flame-dried flask under N_2 were added a stir bar, THF (27 mL, 0.80 M), and diisopropylamine (3.2 mL, 23.10 mmol) and cooled to −78 °C. *N*-butyl lithium (9.2 mL, 23.1 mmol) was slowly added to the reaction flask and stirred vigorously for 15 min. 2-Methylpyridine (**1**) (2.7 mL, 21.0 mmol) was added dropwise over a period of 1 h and allowed to stir for another 1 h before the addition of 1-iodo-2-ethylhexane (3.8 mL, 21.0 mmol) in THF (10 mL, 2.10 M). The reaction was allowed to warm to room temperature overnight. The solvent was concentrated via a rotary evaporator, and the reaction was extracted with dichloromethane and water twice. The organic layer was dried with sodium sulfate, concentrated, and purified by silica gel chromatography using 30% diethylether/hexanes to obtain **2** as a colorless oil (4.45 g, 75%). ^{1}H NMR (300 MHz, $CDCl_3$) δ 8.52 (d, J = 5.0 Hz, 1H), 7.57 (t, J = 7.6 Hz, 1H), 7.14 (d, J = 7.8 Hz, 1H), 7.16−7.05 (m, 1H), 2.79−2.72 (m, 2H), 1.75−1.61 (m, 2H), 1.45−1.20 (m, 9H), and 0.91−0.82 (m, 6H). ^{13}C {^{1}H} NMR (400 MHz, $CDCl_3$) δ 162.9, 149.2, 136.2, 122.5, 120.7, 38.7, 35.8, 33.5, 32.7, 28.9, 25.7, 23.1, 14.1, and 10.8. IR (neat, cm^{-1}): 3067, 3008, 2956, 2924, 2857, 1589, 1568, 1472, 1433, and 747. HRMS (ESI) m/z: $[M]^+$ calcd for $C_{14}H_{23}N$ 205.1830; found 205.1824.

*1-(2-Ethylhexyl)-2-phenylindolizine (**3**).* To a dry flask were added a stir bar, acetone (31 mL, 0.35 M), **2** (2.20 g, 10.7 mmol), and 2-bromo-1-phenylethan-1-one (1.70 g, 8.50 mmol). N_2 was bubbled through the reaction for 5 min, the flask was connected to a reflux condenser, immersed in an oil bath, and refluxed for 6 h. Acetone was evaporated under reduced pressure before $NaHCO_3$ (2.60 g, 31.0 mmol) and H_2O (31 mL, 0.35 M) were added, and the mixture was refluxed again overnight in an oil bath. Dichloromethane was added, and the organic layer was extracted, dried with sodium sulfate, and concentrated under reduced pressure. The product was purified by silica gel chromatography using 10% diethylether/hexanes and 10% ethyl acetate/hexanes to obtain the light brownish thick oily compound **3** (2.10 g, 64%). ^{1}H NMR (300 MHz, $CDCl_3$) δ 7.84 (d, J = 7.0 Hz, 1H), 7.48 (d, J = 6.9 Hz, 2H), 7.40 (t, J = 7.2 Hz, 2H), 7.35−7.27 (m, 3H), 6.62−6.53 (m, 1H), 6.41 (t, J = 6.6 Hz, 1H), 2.79 (m, 2H), 1.44−1.40 (m, 1H), 1.25−1.05 (m, 8H), and 0.81−0.67 (m, 6H). ^{13}C {^{1}H} NMR (400 MHz, $CDCl_3$) δ 136.6, 131.2, 129.6, 129.1, 128.3, 126.3, 124.9, 117.9, 115.7, 110.6, 110.4, 110.0, 40.9, 32.7, 28.8, 28.4, 25.8, 23.1, 14.2, and 10.9. IR (neat, cm^{-1}): 3068, 3031, 2956, 2925, 2856, 1603, 1457, 1369, 1302, 1264, 1211, 734, and 699. HRMS (ESI) m/z: $[M + H]^+$ calcd for $C_{22}H_{27}N$ 306.2222; found 306.2230.

*(Z)-1-(2-Ethylhexyl)-3-((2E,4E)-5-(1-(2-ethylhexyl)-2-phenylindolizin-3-yl)penta-2,4-dien-1-ylidene)-2-phenyl-3H-indolizin-4-ium Perchlorate (**1-EtHxC5**).* To a round-bottom flask equipped with a stir bar were added **3** (2.0 g, 6.55 mmol), acetic anhydride (100 mL, 0.07 M), and perchloric acid (0.8 mL, 2.0 equiv). The flask was flushed with N_2 while stirring for 5 min and then *N*-((1*E*,3*E*,5*E*)-5-(phenylimino)penta-1,3-dien-1-yl)aniline monohydrochloride (0.93 g, 3.25 mmol) was added. The reaction mixture was further stirred for 20 min before triethylamine (2.2 mL, 1.2 equiv) was added and allowed to stir for 24 h at room temperature. Hundred milliliters of DCM and 250 mL of water were added, and the organic layer extracted three times with 100 mL of DCM. The organic layer was dried with sodium sulfate and concentrated via a rotary evaporator. The dye was dissolved in a minimum amount of DCM, and 250 mL of diethylether/hexane (1:1 ratio) was added. The heterogeneous mixture was centrifuged, and the precipitated compound was separated and then dried under vacuum. The solid was subjected to silica gel column chromatography with 20% acetone/80% DCM and 5% MeOH/95% DCM to obtain the green-colored dye **1-EtHxC5** (1.51 g, 69%). Note: this dye is isolated as a mixture of diastereomers. Given the separation of the stereocenters on opposite sides of the π-system, this is expected to have little (or no detectible) influence on

https://doi.org/10.1021/acs.joc.1c01908
J. Org. Chem. 2021, 86, 15376−15386

the optical properties of the dye in the solution. ^{1}H NMR (400 MHz, DMSO-d_6) δ 9.14, (d, J = 7.0 Hz, 2H), 8.00 (d, J = 13.7 Hz, 2H), 7.82 (d, J = 8.7 Hz, 2H), 7.64 (t, J = 7.6 Hz, 4H), 7.58−7.50 (m, 4H), 7.50−7.36 (m, 1H), 7.32 (t, J = 6.7 Hz, 2H), 7.27 (d, J = 7.4 Hz, 4H), 5.69 (t, J = 11.9 Hz, 2H), 2.70−2.55 (m, 4H), 1.11−0.99 (m, 12H), 0.88−0.83 (m, 2H), 0.73 (t, J = 7.4 Hz, 6H), and 0.61 (t, J = 7.5 Hz, 6H). ^{13}C was not obtained due to sparing solubility. IR (neat, cm^{-1}): 3067, 3055, 2954, 2922, 2854,1619, 1560, 1515, 1422, and 961. HRMS (ESI) m/z: $[M]^+$ calcd for $C_{49}H_{57}N_2$ 673.4516; found 673.4535. λ_{max}^{abs} (DCM) = 830 nm. Elemental analysis data was calculated to be C 76.09%, H 7.43%, N 3.62%, and found as C 76.33%, H 7.52%, and N 3.69%.

*4-(2-(3-Ethylheptyl)pyridin-4-yl)-N,N-dimethylaniline (**5**).* To a flask equipped with a stir bar were added 4-bromo-2-(3-ethylheptyl)-pyridine (**4**)[42] (2.50 g, 8.80 mmol), *N*,*N*-dimethyl-4-(4,4,5,5-tetramethyl-1,3,2-dioxaborolan-2-yl)aniline (3.60 g, 12.3 mmol), K_2CO_3 (5.10 g, 37.0 mmol), $Pd(PPh_3)_4$ (0.40 g, 0.35 mmol), and 5:3:3 1,4-dioxane: ethanol: H_2O (44 mL, 0.20 M) under N_2. The reaction flask was immersed in an oil bath and heated to 80 °C for 4 h while monitoring by TLC. The reaction mixture was cooled to room temperature and diluted with H_2O and ethyl acetate. The organic layer was extracted, dried with Na_2SO_4, concentrated, and purified by silica gel column chromatography with 10% ethyl acetate/90% hexanes to obtain **4** as a yellow oil that gradually solidified (2.68 g, 93%). ^{1}H NMR (300 MHz, $CDCl_3$) δ 8.47 (d, J = 6.1 Hz, 1H), 7.57 (d, J = 9.0 Hz, 2H), 7.32 (s, 1H), 7.28−7.26 (m, 1H), 6.79 (d, J = 9.0 Hz, 2H), 3.02 (s, 6H), 2.80 (ap, t, J = 5.4 Hz, 2H), 1.72 (br, s, 2H), 1.39−1.28 (m, 9H), and 0.89−0.86 (m, 6H). ^{13}C {^{1}H} NMR (400 MHz, $CDCl_3$) δ 163.1, 151.0, 149.5, 148.2, 127.7, 125.7, 119.3, 117.8, 112.5, 40.4, 38.9, 36.0, 33.7, 32.8, 28.9, 25.8, 23.2, 14.2, and 10.9. IR (neat, cm^{-1}): 3081, 2955, 2921, 2852, 1595, 1566, 1524, 1443, 1357, and 811. HRMS (ESI) m/z: $[M + H]^+$ calcd for $C_{22}H_{33}N_2$ 325.2644; found 325.2627.

*4-(1-(2-Ethylhexyl)-2-phenylindolizin-7-yl)-N,N-dimethylaniline (**6**).* To a pressure flask equipped with a stir bar were added acetone (25.0 mL, 0.25 M), **5** (2.00 g, 6.16 mmol), and 2-bromo-1-phenylethan-1-one (1.35 g, 6.77 mmol) under N_2. The reaction flask was immersed in an oil bath and heated to reflux for 16 h. The reaction was cooled to room temperature and acetone was evaporated. The oily precipitate was then combined with sodium bicarbonate (2.07 g, 24.6 mmol) and water (25 mL, 0.25 M). The reaction flask was again heated to reflux for 4 h in an oil bath, cooled to room temperature, extracted with dichloromethane, dried with sodium sulfate, and volatiles were evaporated under reduced pressure. The product (**6**) was purified by silica gel chromatography beginning with 100% dichloromethane and then 10% diethylether/ 90% dichloromethane to obtain a yellow solid (1.35 g, 68%).^{1}H NMR (400 MHz, $CDCl_3$) δ 7.87 (d, J = 9.7 Hz, 1H), 7.54 (d, J = 11.8 Hz, 2H), 7.50−7.45 (m, 3H), 7.40 (t, J = 10.1 Hz, 2H), 7.31−7.26 (m, 2H), 6.83 (br, d, J = 11.4 Hz, 2H), 6.72 (dd, J = 2.6 Hz, 9.7 Hz, 1H), 3.00 (s, 6H), 2.84−2.80 (m, 2H), 1.44 (br s, 1H), 1.23−1.18 (m, 8H), and 0.80−0.71 (m, 6H). ^{13}C {^{1}H} NMR (400 MHz, $CDCl_3$) δ 149.8, 136.6, 131.7, 130.2, 129.0, 128.7, 128.3, 126.8, 126.2, 124.8, 113.0, 110.7, 109.8, 109.8, 40.8, 40.7, 32.7, 28.8, 28.5, 25.8, 23.1, 14.1, and 10.9. IR (neat, cm^{-1}): 3055, 3027, 2949, 2923, 2855, 1611, 1525, 1464, 1373, 1359,1167, 813, and 778. HRMS (ESI) m/z: $[M + H]^+$ calcd for $C_{30}H_{37}N_2$ 425.2957; found 425.2935.

*(Z)-7-(4-(Dimethylamino)phenyl)-3-((2E,4E)-5-(7-(4-(dimethylamino)phenyl)-1-(2-ethylhexyl)-2-phenylindolizin-3-yl)-penta-2,4-dien-1-ylidene)-1-(2-ethylhexyl)-2-phenyl-3H-indolizin-4-ium Perchlorate (**7-NMe2PhC5**).* To a round-bottom flask equipped with a stir bar were added **6** (1.20 g, 2.82 mmol), acetic anhydride (28.2 mL, 0.10 M), and perchloric acid (0.20 mL, 2.00 equiv). The flask was flushed with N_2 while stirring for 5 min, and then *N*-((1*E*,3*E*,5*E*)-5-(phenylimino)penta-1,3-dien-1-yl)aniline monohydrochloride (0.40 g, 1.41 mmol) was added. The mixture was further stirred for 20 min before triethylamine (0.50 mL, 1.20 equiv) was added, and the mixture was allowed to stir for 24 h. Five hundred milliliters of 1:2 MeOH: H_2O was added, and the crude product was extracted three times with ethyl acetate. The organic layer was dried with Na_2SO_4 and concentrated via a rotary evaporator. The dye was dissolved in 10 mL of DCM, and 250 mL of diethylether:hexane (3:1 ratio) was added. The heterogeneous mixture was centrifuged, and the precipitated pure compound **7-NMe2PhC5** was dried under vacuum to obtain a greenish-brown solid (1.02 g, 79%). Note: this dye is isolated as a mixture of diastereomers. Given the separation of stereocenters on opposite sides of the π-system, this is expected to have little (or no detectible) influence on the optical properties of the dye in the solution. ^{1}H NMR (400 MHz, DMSO-d_6) δ 8.99 (d, J = 5.5 Hz, 2H), 7.89−7.85 (m, 6H), 7.79 (d, J = 13.0 Hz, 2H), 7.64 (t, J = 7.2 Hz, 2H), 7.58−7.52 (m, 6H), 7.25 (d, J = 7.8 Hz, 4H), 7.09 (t, J = 12.0 Hz, 1H), 6.84 (d, J = 9.1 Hz, 4H), 5.63 (br s, 2H), 3.03 (s, 12H), 2.57 (d, J = 6.2 Hz, 4H), 1.31−1.29 (m, 2H), 1.09−1.03 (m, 16H), 0.74 (t, J = 7.2 Hz, 6H), and 0.61 (t, J = 7.2 Hz, 6H). ^{13}C was not obtained due to sparing solubility. IR (neat, cm^{-1}): 3044, 3026, 2916, 2801, 1590, 1518, 1413, 1128, and 1081. HRMS (ESI) m/z: $[M]^+$ calcd for $C_{65}H_{75}N_4$ 911.5986; found 911.6014. λ_{max}^{abs} (DCM) = 942 nm. Elemental analysis data was calculated to be C 77.16%, H 7.47%, and N 5.54%, and found C 77.29%, H 7.44%, and N 5.57%.

*N,N-Dimethyl-4-(2-phenylindolizin-1-yl)aniline (**8**).* To a flame-dried flask equipped with a stir bar were added acetone (8.4 mL, 0.25 M) and **7** (440 mg, 2.10 mmol).[49] The flask was then purged with N_2 for 10 min. 2-Bromo-1-phenylethan-1-one (460 mg, 2.31 mmol) was added, the flask was sealed, and heated to reflux in an oil bath for 16 h while monitoring by TLC. Upon the disappearance of the starting material, the reaction mixture was cooled to room temperature, the precipitate was then filtered, washed with cool acetone and then combined with sodium bicarbonate (706 mg, 8.40 mmol) dissolved in water (8 mL, 0.25 M). The mixture was heated in a round-bottom flask immersed in an oil bath to reflux for 4 h. The brown precipitate formed was extracted with dichloromethane, dried with sodium sulfate, concentrated, and purified by silica gel column chromatography with 40% dichloromethane/60% hexane to obtain a yellowish-brown solid (**8**) (167 mg, 25%). ^{1}H NMR (400 MHz, CD_3CN) δ 8.07 (d, J = 7.3 Hz, 1H), 7.60 (s, 1H), 7.38−7.24 (m, 6H), 7.13 (d, J = 8.8 Hz, 2H), 6.77 (d, J = 8.8 Hz, 2H), 6.69 (t, J = 6.0 Hz, 1H), 6.54 (t, J = 5.8 Hz, 1H), and 2.95 (s, 6H). ^{13}C {^{1}H} NMR (400 MHz, CD_3CN) δ 149.7, 136.2, 131.3, 129.3, 128.7, 128.1, 126.7, 125.9, 123.3, 117.9, 113.1, 111.9, 111.2, and 40.4. IR (neat, cm^{-1}): 3045, 2794, 1680, 1611, 1535, 1506, 1476, and 1444. HRMS (ESI) m/z: $[M]^+$ calcd for $C_{22}H_{20}N_2$ 312.1626; found 312.1604.

*(Z)-1-(4-(Dimethylamino)phenyl)-3-((2E,4E)-5-(1-(4-(dimethylamino)phenyl)-2-phenylindolizin-3-yl)penta-2,4-dien-1-ylidene)-2-phenyl-3H-indolizin-4-ium Perchlorate (**1-NMe2PhC5**).* To a dry round-bottom flask equipped with a stir bar were added **8** (70 mg, 0.22 mmol), acetic anhydride (2.2 mL, 0.10 M), and perchloric acid (0.01 mL, 2.00 equiv). The flask was flushed with N_2 while stirring for 5 min, and then *N*-((1*E*,3*E*,5*E*)-5-(phenylimino)-penta-1,3-dien-1-yl)aniline monohydrochloride (31.4 mg, 0.11 mmol) was added. The mixture was further stirred for 20 min before triethylamine (0.4 mL, 1.20 equiv) was added and allowed to stir for 24 h at room temperature. Next, 100 mL of diethylether was added, and the heterogeneous mixture was centrifuged to obtain a green precipitate of **1-NMe2PhC5**, which was further washed with diethylether and vacuum dried (54 mg, 72%). ^{1}H NMR (400 MHz, DMSO-d_6) δ 9.25 (d, J = 9.5 Hz, 2H), 8.08 (d, J = 18.4 Hz, 2H), 7.76 (d, J = 11.4 Hz, 2H), 7.66 (t, J = 8.9 Hz, 2H), 7.58−7.56 (m, 2H), 7.45 (t, J = 10.5 Hz, 4H), 7.39 (t, J = 11.0 Hz, 2H), 7.29−7.23 (m, 5H), 7.06 (d, J = 11.7 Hz, 4H), 6.66 (d, J = 12.0 Hz, 4H), 5.69 (d, J = 17.6 Hz, 2H), and 2.89 (s, 12H). ^{13}C was not obtained due to sparing solubility. IR (neat, cm^{-1}): 3020, 2989, 2822, 2802, 1608, 1512, and 1082. HRMS (ESI) m/z: calcd for $C_{49}H_{43}N_4$ $[M]^+$ 687.3488; found 687.3428. λ_{max}^{abs} (DCM) = 894 nm. An HPLC trace is provided in Figure S13. We note that the HPLC detection system is absorption-based and without knowing the molar absorptivity of any impurities knowing the exact percent purity of the sample is not possible. The chromatograph indicates that at 900 nm where **1-NMe$_2$PhC5** absorbs strongly peak areas are 98% dye using a gradient-mobile phase of 75% MeOH/25% H_2O transitioning to 100% MeOH and a 0.5 mL/min

https://doi.org/10.1021/acs.joc.1c01908
J. Org. Chem. 2021, 86, 15376−15386

flow rate. The same peak area is observed when monitoring signals at 254 nm, where many common impurities absorb.

*(4-Bromopyridin-2-yl)(4-(dimethylamino)phenyl)methanol (**10**).* To a flask equipped with a stir bar were added Mg turning (0.38 g, 15.60 mmol), tetrahydrofuran (38 mL, 0.40 M), two drops of 1,2-dibromoethane, and 4-bromo-*N*,*N*-dimethylaniline (3.00 g, 15.0 mmol) under N_2. The flask was immersed in a 40 °C oil bath and heated until near-complete consumption of the Mg turnings. Next, the Grignard reagent mixture was cooled to room temperature still under N_2. To a second flask equipped with a stir bar were added tetrahydrofuran (35 mL, 0.43 M) and 4-bromo-2-formylpyridine (**9**) (2.80 g, 15.0 mmol). The mixture was then cooled to −78 °C. The prepared Grignard reagent was added dropwise to the second flask at −78 °C via syringe and allowed to warm to room temperature with stirring overnight. Next, 100 mL of saturated aqueous ammonium chloride was added to the reaction mixture, and the mixture was stirred for 10 min. Dichloromethane was added, then the organic layer extracted, dried with sodium sulfate, and evaporated under reduced pressure. The product (**10**) was purified by silica gel chromatography using a gradient of 10−20% acetone/90−80% dichloromethane to obtain a yellow solid (1.90 g, 58%). ^{1}H NMR (400 MHz, $CDCl_3$) δ 8.36 (d, J = 5.2 Hz, 1H), 7.39 (s, 1H), 7.33 (d, J = 5.2 Hz, 1H), 7.20 (d, J = 8.8 Hz, 2H), 6.70 (d, J = 8.8 Hz, 2H), 5.65 (s, 1H), 4.58 (s, 1H), and 2.94 (s, 6H). ^{13}C {^{1}H} NMR (400 MHz, $CDCl_3$) δ 163.7, 150.5, 148.7, 133.5, 130.2, 128.1, 125.6, 124.6, 112.6, 74.9, and 40.5. IR (neat, cm^{-1}): 3173 (br), 3064, 2885, 2798, 1612, 1571, 1519, 1462, 1389, 1313, 1209, 1058, and 805. HRMS (ESI) m/z: $[M + H]^+$ calcd for $C_{14}H_{16}N_2BrO$ 307.0446; found 307.0410.

*4-((4-Bromopyridin-2-yl)methyl)-N,N-dimethylaniline (**11**).* To a flask equipped with a stir bar were added **10** (2.00 g, 6.50 mmol), glacial acetic acid (22 mL, 0.30 M), and aqueous hydriodic acid (2.2 mL, 29.0 mmol). The reaction flask was immersed in an oil bath and heated to 120 °C for 2.5 h while monitoring by TLC. Once the starting material was completely consumed, the mixture was cooled to room temperature, 100 mL of saturated aqueous sodium sulfite (Na_2SO_3) was added, and the mixture was stirred for 10 min. The reaction was neutralized with 1.0 M aqueous NaOH, 100 mL of dichloromethane was added, and the organic layer was extracted. The organic layer was dried with sodium sulfate, evaporated under reduced pressure, and the product purified by silica gel chromatography using 15% ethyl acetate/85% dichloromethane to obtain a yellow solid (**11**) (1.18 g, 62%). Note: a minor impurity could not be removed, and the mixture was carried forward directly. ^{1}H NMR (300 MHz, $CDCl_3$) δ 8.18 (d, J = 5.9 Hz, 1H), 7.49−7.46 (m, 2H), 7.13 (s, J = 8.7 Hz, 2H), 6.73 (d, J = 8.7 Hz, 2H), 4.00 (s, 2H), and 2.93 (s, 6H). ^{13}C {^{1}H} NMR (400 MHz, $CDCl_3$) δ 162.9, 149.5, 132.3, 130.4, 129.8, 126.3, 124.5, 113.2, 106.2, 43.4, and 40.9. Regarding the ^{13}C NMR, it is important to note that a minor impurity is present in this spectrum, and the most intense peaks have been reported here; however, since this material was carried forward with this impurity synthetically, there are additional peaks in the spectrum that could not be removed. Due to relaxation times of ^{13}C being nonreliable with this NMR setup, these peaks above could have impurity contributions. The spectrum is only reported as a general reference. IR (neat, cm^{-1}): 2912, 2803, 1614, 1562, 1520, 1355, 1212, and 800. HRMS (ESI) m/z: $[M + H]^+$ calcd for $C_{14}H_{15}N_2Br$ 291.0497; found 291.0505.

*4-(2-(4-(Dimethylamino)benzyl)pyridin-4-yl)-N,N-dimethylaniline (**12**).* To a flask under N_2 were added a stir bar, **11** (1.00 g, 3.44 mmol), *N*,*N*-dimethyl-4-(4,4,5,5-tetramethyl-1,3,2-dioxaborolan-2-yl)aniline (1.02 g, 4.13 mmol), $Pd(PPh_3)_4$ (0.20 g, 0.17 mmol), K_2CO_3 (0.95 g, 6.88 mmol), and 3:3:7 ethanol/water/1,4-dioxane (17 mL, 0.20 M). The reaction flask was submerged in an oil bath and heated to 80°C for 12 h. Next, the reaction was cooled to room temperature, 100 mL of ethyl acetate was added, the organic layer was extracted, and the organic layer was washed three times with 100 mL of water. The organic layer was dried with sodium sulfate, concentrated under reduced pressure, and the product was purified by quick silica gel chromatography using 10% acetone/90% dichloromethane to obtain a golden-yellow solid (**12**) (0.85 g, 74%). ^{1}H NMR (300 MHz, $CDCl_3$) δ 8.48 (d, J = 6.3 Hz, 1H), 7.51 (d, J = 9.0 Hz, 2H), 7.30−7.20 (m, 2H), 7.19 (d, J = 8.8 Hz, 2H), 6.76−6.69 (m, 4H), 4.10 (s, 2H), 3.00 (s, 6H), and 2.91 (s, 6H). Note: a minor impurity is present as shown in ^{1}H NMR at ∼7.6 ppm. This impurity was carried forward without further purification since a 2D TLC shows the compound decomposes at an appreciable rate on silica gel. The impurity was removed in the following step. IR (neat, cm^{-1}): 3012, 2993, 2893, 2813, 2801, 1609, 1589, 1562, 1520, 1469, 1366, 1347, 1207, and 807. HRMS (ESI) m/z: $[M + H]^+$ calcd for $C_{22}H_{26}N_3$ 332.2127; found 332.2112.

*4,4′-(2-Phenylindolizine-1,7-diyl)bis(N,N-dimethylaniline) (**13**).* To a flask equipped with a stir bar were added acetone (9 mL, 0.25 M), **12** (0.72 g, 2.17 mmol), and 2-bromo-1-phenylethan-1-one (0.48 g, 2.39 mmol) under N_2. The reaction flask was immersed in an oil bath and heated to reflux for 16 h. The mixture was cooled to room temperature, and the precipitate was filtered, washed with additional acetone, and then combined with sodium bicarbonate (0.73 g, 8.68 mmol) and water (25 mL, 0.09 M). The reaction flask was again submerged in an oil bath and heated to reflux for 4 h, cooled to room temperature, extracted with dichloromethane, dried with sodium sulfate, and evaporated under reduced pressure. The mixture was purified by alumina column chromatography using 80% dichloromethane/20% hexane to obtain a yellow fluorescent solid (**13**) (0.50 g, 53%). ^{1}H NMR (300 MHz, $CDCl_3$) δ 7.85 (d, J = 7.2 Hz, 1H), 7.54 (s, 1H), 7.43 (d, J = 8.9 Hz, 2H), 7.33 (s, 1H), 7.28 (d, J = 6.8 Hz, 2H), 7.23−7.14 (m, 5H), and 6.78 (m, 4H). ^{13}C {^{1}H} NMR (400 MHz, $CDCl_3$) δ 149.8, 148.6, 135.7, 131.0, 130.2, 129.8, 129.0, 128.2, 127.9, 126.8, 126.1, 124.9, 123.5, 113.3, 113.1, 112.8, 112.7, 112.4, 110.6, 110.4, 40.7, and 40.6. IR (neat, cm^{-1}): 3025, 2980, 2882, 2848, 2795, 1607, 1522, 1476, 1441, 1346, 943, 814, 769, and 696. HRMS (ESI) m/z: $[M]^+$ calcd for $C_{30}H_{29}N_3$ 431.2361; found 431.2351.

*(Z)-3-((2E,4E)-5-(1,7-Bis(4-(dimethylamino)phenyl)-2-phenylindolizin-3-yl)penta-2,4-dien-1-ylidene)-1,7-bis(4-(dimethylamino)-phenyl)-2-phenyl-3H-indolizin-4-ium Perchlorate (**1,7-NMe2PhC5**).* To a dry flask equipped with a stir bar were added **13** (130 mg, 0.30 mmol), acetic anhydride (6 mL, 0.05 M), and perchloric acid (0.02 mL, 2.00 equiv). The flask was flushed with N_2 while stirring for 5 min, and then *N*-((1*E*,3*E*,5*E*)-5-(phenylimino)-penta-1,3-dien-1-yl)aniline monohydrochloride (43 mg, 0.15 mmol) was added. The mixture was further stirred for 20 min before triethylamine (0.10 mL, 1.20 equiv) was added, and the mixture was allowed to stir for 24 h at room temperature. Next, 100 mL of diethylether was added, and the precipitate was centrifuged to obtain a brown solid. The solid was purified by silica gel chromatography with 100% DCM, 20% acetone/80% DCM, and then 5% propanol/95% DCM to obtain the pure compound **1,7-NMe2PhC5** (20 mg, 13%). ^{1}H NMR (400 MHz, DMSO-d_6) δ 9.05 (d, J = 9.8 Hz, 2H), 7.84 (d, J = 18.4 Hz, 2H), 7.72−7.69 (m, 5H), 7.62−7.55 (m, 4H), 7.45 (t, J = 9.8 Hz, 4H), 7.24 (d, J = 9.2 Hz, 4H), 7.17−7.06 (m, 2H), 7.07 (d, J = 11.8 Hz, 4H), 6.80 (d, J = 12.2 Hz, 4H), 6.65 (d, J = 11.8 Hz, 4H), 5.66 (t, J = 17.1 Hz, 2H), and 3.01 (s, 12H), 2.90 (s, 12H). ^{13}C was not found because of sparing solubility. IR (neat, cm^{-1}): 3360, 3194, 2920, 2854, 1594, 1514, 1484, 1442, 1144, and 1094. HRMS (ESI) m/z: $[M]^+$ calcd for $C_{65}H_{61}N_6$ 925.4952; found 925.4960. λ_{max}^{abs} (DCM) = 994 nm. An HPLC trace is provided in Figure S15. We note that the HPLC detection system is absorption-based, and without knowing the molar absorptivity of any impurities knowing the exact percent purity of the sample is not possible. The chromatograph indicates that at 949 nm where **1,7-NMe$_2$PhC5** absorbs strongly, the observed peak area is 100% dye using a 100% acetone mobile phase and a 0.5 mL/min flow rate. A slight shoulder is observed just before the dye peak, but the shoulder was too small to allow for integration with the instrument used. Notably, 949 nm is the longest wavelength observable in our system. A 90% dye peak area is observed when monitoring signals at 254 nm, where many common impurities absorb. We note that at 949 nm there is no background signal from the solvent, but at 254 nm, there is some background from the solvent at this wavelength that could lead to poor integration (Figure S16). We note that the peak for the dye is present at an early retention time. Efforts to change solvent to mixed systems, gradual mobility phase changing systems, flow rates, and numerous organic

https://doi.org/10.1021/acs.joc.1c01908
J. Org. Chem. 2021, 86, 15376−15386

soluble phases attempted led to severe streaking of this material in our experience.

Encapsulation Procedures and Data. *(a). Dye Encapsulation with PAMAM-PCL.* The dye (**1,7-NMe2PhC5**) was encapsulated with PAMAM-PCL following the literature procedure.[40] Briefly, **1,7-NMe2PhC5** (1 mg) and PAMAM-PCL (2 mg) were dissolved in 200 μL of THF and added dropwise to 2 mL of MilliQ water while stirring and sonicating for 5 min. The sample was placed under a stream of nitrogen to remove THF by allowing it to evaporate. The formulations were allowed to equilibrate for 12 h, and the unloaded dye was filtered out using a 0.45 μm syringe filter. The encapsulated dye with PAMAM-PCL was then used for these studies.

(b). Dye-DSPE-mPG2000 Micelle. A modified film hydration technique was used to prepare the sample following literature procedures.[19] A 4 mL of 1.0×10^{-3} M solution of **1,7-NMe2PhC5** in chloroform was prepared to make the dye stock solution. Fifty milligrams of DSPE-mPEG2000 was dissolved in 2 mL of chloroform in another vial to form the DSPE-mPEG2000 stock solution. Twenty microliters of the dye solution was dissolved in 1.2 mL of the DSPE-mPEG2000 stock solution, and the mixture was swirled until homogeneity was attained. The Dye-DSPE-mPEG2000 mixture in chloroform was concentrated at room temperature under vacuum until chloroform was mostly evaporated. The mixture was further concentrated using a rotary evaporation at 55 °C for 3 h to make sure that the mixture was chloroform free. Two milliliters of DI water was then added to the Dye-DSPE-mPEG2000 paste mixture, and the mixture was stirred for 10 min while warming at 50 °C to ensure the sample dissolved. The mixture was further sonicated for 1 min to completely solubilized any undissolved particles, forming the Dye-DSPE-mPEG2000 micelle, which was used directly.

(c). Dye-PF-127 Micelle. The encapsulation procedure was carried out following a modified literature procedure.[41] One hundred milligrams of pluronic F-127 (PF-127) was dissolved in 2 mL of chloroform, stirred, and sonicated until the sample was completely solubilized. Fifty microliters of a 1.0×10^{-3} M solution of **1,7-NMe2PhC5** in chloroform was added to the 2 mL PF-127 solution, and the mixture was stirred until homogeneity was attained. The Dye-PF-127 chloroform solution was rotary evaporated at 50 °C for 3 h. We note that this drying time is critical to the aggregation state of the dye and the stability of the dye-encapsulated nanoparticles over time. If the complete drying of chloroform is not obtained, then mostly the blue-shifted (consistent with H-aggregate) material is observed via absorption spectroscopy. If even small amounts of chloroform remain, dye-encapsulated nanoparticles will be stable only on the hour time scale in a deaggregated state with aggregates gradually forming (Figure S7). If complete dryness is reached, dye-encapsulated nanoparticles were stable for more than a month stored in a water solution (Figure S8). DI water (3 mL) was then added to the Dye-PF-127 paste, stirred while warming for 20 min, and then sonicated for 1 min to solubilize the remaining undissolved particles. The mixture was then used directly in the studies.

■ ASSOCIATED CONTENT

Supporting Information

The Supporting Information is available free of charge at https://pubs.acs.org/doi/10.1021/acs.joc.1c01908.

Encapsulation data and graphs, computational data, photophysical data, HPLC chromatogram traces, and ^{1}H and ^{13}C NMR spectra of intermediates and final compounds (PDF)

■ AUTHOR INFORMATION

Corresponding Author

Jared H. Delcamp − *Department of Chemistry and Biochemistry, University of Mississippi, University, Mississippi 38677, United States;* orcid.org/0000-0001-5313-4078; Email: delcamp@olemiss.edu

Authors

David Ndaleh − *Department of Chemistry and Biochemistry, University of Mississippi, University, Mississippi 38677, United States;* orcid.org/0000-0001-6705-6197

Cameron Smith − *Department of Chemistry and Biochemistry, University of Mississippi, University, Mississippi 38677, United States;* orcid.org/0000-0003-3072-028X

Mahesh Loku Yaddehige − *Department of Chemistry and Biochemistry, University of Mississippi, University, Mississippi 38677, United States;* orcid.org/0000-0003-2732-9706

Abdul Kalam Shaik − *Department of Chemistry and Biochemistry, University of Mississippi, University, Mississippi 38677, United States;* orcid.org/0000-0001-9704-9254

Davita L. Watkins − *Department of Chemistry and Biochemistry, University of Mississippi, University, Mississippi 38677, United States;* orcid.org/0000-0002-0943-7220

Nathan I. Hammer − *Department of Chemistry and Biochemistry, University of Mississippi, University, Mississippi 38677, United States;* orcid.org/0000-0002-6221-2709

Complete contact information is available at: https://pubs.acs.org/10.1021/acs.joc.1c01908

Author Contributions

The manuscript was written through the contributions of all authors. All authors have given approval to the final version of the manuscript.

Notes

The authors declare no competing financial interest.

■ ACKNOWLEDGMENTS

The authors thank the National Science Foundation for funding this work through award 1757220.

■ REFERENCES

(1) Zhao, J.; Zhong, D.; Zhou, S. NIR-I-to-NIR-II fluorescent nanomaterials for biomedical imaging and cancer therapy. *J. Mater. Chem. B* **2018**, *6*, 349−365.

(2) Jin, T. Review—Recent Progress in NIR Fluorophores Emitting over 1000 nm for Bioimaging. *ECS J. Solid State Sci. Technol.* **2019**, *8*, R9−R13.

(3) Wang, Q.; Dai, Y.; Xu, J.; Cai, J.; Niu, X.; Zhang, L.; Chen, R.; Shen, Q.; Huang, W.; Fan, Q. All-in-One Phototheranostics: Single Laser Triggers NIR-II Fluorescence/Photoacoustic Imaging Guided Photothermal/Photodynamic/Chemo Combination Therapy. *Adv. Funct. Mater.* **2019**, *29*, No. 1901480.

(4) Zhu, S.; Tian, R.; Antaris, A. L.; Chen, X.; Dai, H. Near-Infrared-II Molecular Dyes for Cancer Imaging and Surgery. *Adv. Mater.* **2019**, *31*, No. 1900321.

(5) Dai, H.; Shen, Q.; Shao, J.; Wang, W.; Gao, F.; Dong, X. Small Molecular NIR-II Fluorophores for Cancer Phototheranostics. *The Innovation* **2021**, *2*, No. 100082.

(6) Wang, R.; Li, X.; Yoon, J. Organelle-Targeted Photosensitizers for Precision Photodynamic Therapy. *ACS Appl. Mater. Interfaces* **2021**, *13*, 19543−19571.

(7) Schnermann, M. J. Organic dyes for deep bioimaging. *Nature* **2017**, *551*, 176−177.

(8) Shindy, H. A. Fundamentals in the chemistry of cyanine dyes: A review. *Dyes Pigm.* **2017**, *145*, 505−513.

(9) Feng, L.; Chen, W.; Ma, X.; Liu, S. H.; Yin, J. Near-infrared heptamethine cyanines (Cy7): from structure, property to application. *Org. Biomol. Chem.* **2020**, *18*, 9385−9397.
(10) Usama, S. M.; Burgess, K. Hows and Whys of Tumor-Seeking Dyes. *Acc. Chem. Res.* **2021**, *54*, 2121−2131.
(11) Yang, X. Z.; Xu, B.; Shen, L.; Sun, R.; Xu, Y. J.; Song, Y. L.; Ge, J. F. Series of Mitochondria/Lysosomes Self-Targetable Near-Infrared Hemicyanine Dyes for Viscosity Detection. *Anal. Chem.* **2020**, *92*, 3517−3521.
(12) Ashitate, Y.; Levitz, A.; Park, M. H.; Hyun, H.; Venugopal, V.; Park, G.; El Fakhri, G.; Henary, M.; Gioux, S.; Frangioni, J. V.; Choi, H. S. Endocrine-specific NIR fluorophores for adrenal gland targeting. *Chem. Commun.* **2016**, *52*, 10305−10308.
(13) Siriwibool, S.; Kaekratoke, N.; Chansaenpak, K.; Siwawannapong, K.; Panajapo, P.; Sagarik, K.; Noisa, P.; Lai, R. Y.; Kamkaew, A. Near-Infrared Fluorescent pH Responsive Probe for Targeted Photodynamic Cancer Therapy. *Sci. Rep.* **2020**, *10*, No. 1283.
(14) Cosco, E. D.; Caram, J. R.; Bruns, O. T.; Franke, D.; Day, R. A.; Farr, E. P.; Bawendi, M. G.; Sletten, E. M. Flavylium Polymethine Fluorophores for Near- and Shortwave Infrared Imaging. *Angew. Chem., Int. Ed.* **2017**, *56*, 13126−13129.
(15) Cosco, E. D.; Arus, B. A.; Spearman, A. L.; Atallah, T. L.; Lim, I.; Leland, O. S.; Caram, J. R.; Bischof, T. S.; Bruns, O. T.; Sletten, E. M. Bright Chromenylium Polymethine Dyes Enable Fast, Four-Color In Vivo Imaging with Shortwave Infrared Detection. *J. Am. Chem. Soc.* **2021**, *143*, 6836−6846.
(16) Pengshung, M.; Li, J.; Mukadum, F.; Lopez, S. A.; Sletten, E. M. Photophysical Tuning of Shortwave Infrared Flavylium Heptamethine Dyes via Substituent Placement. *Org. Lett.* **2020**, *22*, 6150−6154.
(17) Li, B.; Zhao, M.; Feng, L.; Dou, C.; Ding, S.; Zhou, G.; Lu, L.; Zhang, H.; Chen, F.; Li, X.; Li, G.; Zhao, S.; Jiang, C.; Wang, Y.; Zhao, D.; Cheng, Y.; Zhang, F. Organic NIR-II molecule with long blood half-life for in vivo dynamic vascular imaging. *Nat. Commun.* **2020**, *11*, No. 3102.
(18) Wang, S.; Fan, Y.; Li, D.; Sun, C.; Lei, Z.; Lu, L.; Wang, T.; Zhang, F. Anti-quenching NIR-II molecular fluorophores for in vivo high-contrast imaging and pH sensing. *Nat. Commun.* **2019**, *10*, No. 1058.
(19) Lei, Z.; Sun, C.; Pei, P.; Wang, S.; Li, D.; Zhang, X.; Zhang, F. Stable, Wavelength-Tunable Fluorescent Dyes in the NIR-II Region for In Vivo High-Contrast Bioimaging and Multiplexed Biosensing. *Angew. Chem., Int. Ed.* **2019**, *58*, 8166−8171.
(20) Li, B.; Lu, L.; Zhao, M.; Lei, Z.; Zhang, F. An Efficient 1064 nm NIR-II Excitation Fluorescent Molecular Dye for Deep-Tissue High-Resolution Dynamic Bioimaging. *Angew. Chem., Int. Ed.* **2018**, *57*, 7483−7487.
(21) Ding, B.; Xiao, Y.; Zhou, H.; Zhang, X.; Qu, C.; Xu, F.; Deng, Z.; Cheng, Z.; Hong, X. Polymethine Thiopyrylium Fluorophores with Absorption beyond 1000 nm for Biological Imaging in the Second Near-Infrared Subwindow. *J. Med. Chem.* **2019**, *62*, 2049−2059.
(22) Gayton, J. N.; Autry, S.; Fortenberry, R. C.; Hammer, N. I.; Delcamp, J. H. Counter Anion Effect on the Photophysical Properties of Emissive Indolizine-Cyanine Dyes in Solution and Solid State. *Molecules* **2018**, *23*, 3051.
(23) Gayton, J.; Autry, S. A.; Meador, W.; Parkin, S. R.; Hill, G. A.; Hammer, N. I.; Delcamp, J. H. Indolizine-Cyanine Dyes: Near Infrared Emissive Cyanine Dyes with Increased Stokes Shifts. *J. Org. Chem.* **2019**, *84*, 687−697.
(24) Lee, C.; Yang, W.; Parr, R. G. Development of the Colle-Salvetti correlation-energy formula into a functional of the electron density. *Phys. Rev. B* **1988**, *37*, 785−789.
(25) Becke, A. D. Density-functional thermochemistry. III. The role of exact exchange. *J. Chem. Phys.* **1993**, *98*, 5648−5652.
(26) Frisch, M. J.; Pople, J. A.; Binkley, J. S. Self-consistent molecular orbital methods 25. Supplementary functions for Gaussian basis sets. *J. Chem. Phys.* **1984**, *80*, 3265−3269.
(27) Miertuš, S.; Scrocco, E.; Tomasi, J. Electrostatic Interaction of a Solute with a Continuum. A Direct Utilization of Ab Initio Molecular Potentials for the Prevision of Solvent Effects. *Chem. Phys.* **1981**, *55*, 117−129.
(28) Miertus, S.; Tomasi, J. Approximate Evaluations of the Electrostatic Free Energy and Internal Energy Changes in Solution Processes. *Chem. Phys.* **1982**, *65*, 239−245.
(29) Pascual-Ahuir, J. L.; Silla, E.; Tunon, I. GEPOL: An Improved Description of Molecular Surfaces. III. A New Algorithm for the Computation of a Solvent-Excluding Surface. *J. Comput. Chem.* **1994**, *15*, 1127−1138.
(30) Mustroph, H.; Towns, A. Fine Structure in Electronic Spectra of Cyanine Dyes: Are Sub-Bands Largely Determined by a Dominant Vibration or a Collection of Singly Excited Vibrations? *ChemPhysChem* **2018**, *19*, 1016−1023.
(31) Wallace, A. M.; Curiac, C.; Delcamp, J. H.; Fortenberry, R. C. Accurate determination of the onset wavelength (λonset) in optical spectroscopy. *J. Quant. Spectrosc. Radiat. Transfer* **2021**, *265*, No. 107544.
(32) Reindl, S.; Penzkofer, A.; Gong, S.-H.; Landthaler, M.; Szeimies, R. M.; Abels, C.; Bäumler, W. Quantum Yield of Triplet Formation for Indocyanine Green. *J. Photochem. Photobio. A* **1997**, *105*, 65−68.
(33) Alander, J. T.; Kaartinen, I.; Laakso, A.; Patila, T.; Spillmann, T.; Tuchin, V. V.; Venermo, M.; Välisuo, P. A review of indocyanine green fluorescent imaging in surgery. *Int. J. Biomed. Imaging* **2012**, *2012*, No. 940585.
(34) Yan, J. W.; Zhu, J. Y.; Zhou, K. X.; Wang, J. S.; Tan, H. Y.; Xu, Z. Y.; Chen, S. B.; Lu, Y. T.; Cui, M. C.; Zhang, L. Neutral merocyanine dyes: for in vivo NIR fluorescence imaging of amyloid-beta plaques. *Chem. Commun.* **2017**, *53*, 9910−9913.
(35) Zhang, C.; Long, L.; Chunmeng, S. Mitochontria-Targeting IR-780 Dye and Its Derivatives. Synthesis, Mechanisms of Action, and Theranostic Applications. *Adv. Ther.* **2018**, *1*, No. 1800069.
(36) Prajapati, S. I.; Martinez, C. O.; Bahadur, A. N.; Wu, I. Q.; Zheng, W.; Lechleiter, J. D.; McManus, L. M.; Chisholm, G. B.; Michalek, J. E.; Shireman, P. K.; Keller, C. Near-Infrared Imaging of Injured Tissue in Living Subjects Using IR-820. *Mol. Imaging* **2009**, *8*, 45−54.
(37) James, N. S.; Chen, Y.; Joshi, P.; Ohulchanskyy, T. Y.; Ethirajan, M.; Henary, M.; Strekowsk, L.; Pandey, R. K. Evaluation of polymethine dyes as potential probes for near infrared fluorescence imaging of tumors: part - 1. *Theranostics* **2013**, *3*, 692−702.
(38) Casalboni, M.; De Matteis, F.; Prosposito, P.; Quatela, A.; Sarcinelli, F. Fluorescence efficiency of four infrared polymethine dyes. *Chem. Phys. Lett.* **2003**, *373*, 372−378.
(39) Antaris, A. L.; Chen, H.; Cheng, K.; Sun, Y.; Hong, G.; Qu, C.; Diao, S.; Deng, Z.; Hu, X.; Zhang, B.; Zhang, X.; Yaghi, O. K.; Alamparambil, Z. R.; Hong, X.; Cheng, Z.; Dai, H. A small-molecule dye for NIR-II imaging. *Nat. Mater.* **2016**, *15*, 235−242.
(40) Chandrasiri, I.; Abebe, D. G.; Loku Yaddehige, M.; Williams, J. S. D.; Zia, M. F.; Dorris, A.; Barker, A.; Simms, B. L.; Parker, A.; Vinjamuri, B. P.; Le, N.; Gayton, J. N.; Chougule, M. B.; Hammer, N. I.; Flynt, A.; Delcamp, J. H.; Watkins, D. L. Self-Assembling PCL−PAMAM Linear Dendritic Block Copolymers (LDBCs) for Bioimaging and Phototherapeutic Applications. *ACS Appl. Bio Mater.* **2020**, *3*, 5664−5677.
(41) Sreejith, S.; Joseph, J.; Lin, M.; Menon, N. V.; Borah, P.; Ng, H. J.; Loong, Y. X.; Kang, Y.; Yu, S. W.-K.; Zhao, Y. Near-Infrared Squaraine Dye Encapsulated Micelles for in Vivo Fluorescence and Photoacoustic Bimodal Imaging. *ACS Nano* **2015**, *9*, 5695−5704.
(42) Huckaba, A. J.; Yella, A.; Brogdon, P.; Murphy, J. S.; Nazeeruddin, M. K.; Grätzel, M.; Delcamp, J. H. A Low Recombination Rate Indolizine Sensitizer for Dye-Sensitized Solar Cells. *Chem. Commun.* **2016**, *52*, 8424−8427.
(43) Parker, C. A.; Rees, W. T. Correction of Fluorescence Spectra and Measurement of Fluorescence Quantum Efficiency. *Analyst* **1960**, *85*, 587−600.

https://doi.org/10.1021/acs.joc.1c01908
J. Org. Chem. 2021, 86, 15376−15386

(44) Benson, R. C.; Kues, H. A. Fluorescence Properties of Indocyanine Green as Related to Angiography. *Phys. Med. Biol.* **1978**, *23*, 159−163.
(45) Würth, C.; Grabolle, M.; Pauli, J.; Spieles, M.; Resch-Genger, U. Comparison of methods and achievable uncertainties for the relative and absolute measurement of photoluminescence quantum yields. *Anal. Chem.* **2011**, *83*, 3431−3439.
(46) Frisch, M. J.; Trucks, G. W.; Schlegel, H. B.; Scuseria, G. E.; Robb, M. A.; Cheeseman, J. R.; Scalmani, G.; Barone, V.; Petersson, G. A.; Nakatsuji, H.; Li, X.; Caricato, M.; Marenich, A. V.; Bloino, J.; Janesko, B. G.; Gomperts, R.; Mennucci, B.; Hratchian, H. P.; Ortiz, J. V.; Izmaylov, A. F.; Sonnenberg, J. L.; Williams-Young, D.; Ding, F.; Lipparini, F.; Egidi, F.; Goings, J.; Peng, B.; Petrone, A.; Henderson, T.; Ranasinghe, D.; Zakrzewski, V. G.; Gao, J.; Rega, N.; Zheng, G.; Liang, W.; Hada, M.; Ehara, M.; Toyota, K.; Fukuda, R.; Hasegawa, J.; Ishida, M.; Nakajima, T.; Honda, Y.; Kitao, O.; Nakai, H.; Vreven, T.; Throssell, K.; Montgomery, J. A., Jr.; Peralta, J. E.; Ogliaro, F.; Bearpark, M. J.; Heyd, J. J.; Brothers, E. N.; Kudin, K. N.; Staroverov, V. N.; Keith, T. A.; Kobayashi, R.; Normand, J.; Raghavachari, K.; Rendell, A. P.; Burant, J. C.; Iyengar, S. S.; Tomasi, J.; Cossi, M.; Millam, J. M.; Klene, M.; Adamo, C.; Cammi, R.; Ochterski, J. W.; Martin, R. L.; Morokuma, K.; Farkas, O.; Foresman, J. B.; Fox, D. J. *Gaussian 16*, revision: A.03; Gaussian, Inc.: Wallingford CT, 2016.
(47) Hehre, W. J.; Ditchfield, R.; Pople, J. A. Self—Consistent Molecular Orbital Methods. XII. Further Extensions of Gaussian—Type Basis Sets for Use in Molecular Orbital Studies of Organic Molecules. *J. Chem. Phys.* **1972**, *56*, 2257−2261.
(48) Francl, M. M.; Pietro, W. J.; Hehre, W. J.; Binkley, J. S.; Gordon, M. S.; DeFrees, D. J.; Pople, J. A. Self-consistent molecular orbital methods. XXIII. A polarization-type basis set for second-row elements. *J. Chem. Phys.* **1982**, *77*, 3654−3665.
(49) Yang, S.; Tang, W.; Yang, Z.; Xu, J. Iridium-Catalyzed Highly Efficient and Site-Selective Deoxygenation of Alcohols. *ACS Catal.* **2018**, *8*, 9320−9326.

NOTE ADDED AFTER ASAP PUBLICATION

Revisions were made to the original posting of this article. The value in the abstract was revised and an error was corrected in the caption of Figure 4. The corrected article published October 15, 2021.

https://doi.org/10.1021/acs.joc.1c01908
J. Org. Chem. 2021, 86, 15376−15386